Springer

Dear Author

Here are the proofs of your article.

- You can submit your corrections **online,** via **e-mail** or by **fax**.
- For **online** submission please insert your corrections in the online correction form. Always indicate the line number to which the correction refers.
- You can also insert your corrections in the proof PDF and **email** the annotated PDF.
- For **fax** submission, please ensure that your corrections are clearly legible. Use a fine black pen and write the correction in the margin, not too close to the edge of the page.
- Remember to note the **journal title**, **article number**, and **your name** when sending your response via e-mail or fax.
- **Check** the metadata sheet to make sure that the header information, especially author names and the corresponding affiliations are correctly shown.
- **Check** the questions that may have arisen during copy editing and insert your answers/corrections.
- **Check** that the text is complete and that all figures, tables and their legends are included. Also check the accuracy of special characters, equations, and electronic supplementary material if applicable. If necessary refer to the *Edited manuscript*.
- The publication of inaccurate data such as dosages and units can have serious consequences. Please take particular care that all such details are correct.
- Please **do not** make changes that involve only matters of style. We have generally introduced forms that follow the journal's style.
- Substantial changes in content, e.g., new results, corrected values, title and authorship are not allowed without the approval of the responsible editor. In such a case, please contact the Editorial Office and return his/her consent together with the proof.
- If we do not receive your corrections **within 48 hours**, we will send you a reminder.
- Your article will be published **Online First** approximately one week after receipt of your corrected proofs. This is the **official first publication** citable with the DOI. **Further changes are, therefore, not possible.**
- The **printed version** will follow in a forthcoming issue.

Please note

After online publication, subscribers (personal/institutional) to this journal will have access to the complete article via the DOI using the URL:

`http://dx.doi.org/10.1007/s00367-017-0492-8`

If you would like to know when your article has been published online, take advantage of our free alert service. For registration and further information, go to: http://www.link.springer.com.

Due to the electronic nature of the procedure, the manuscript and the original figures will only be returned to you on special request. When you return your corrections, please inform us, if you would like to have these documents returned.

AUTHOR'S PROOF!

Metadata of the article that will be visualized in OnlineFirst

1	Article Title	**Probabilistic stability evaluation and seismic triggering scenarios of submerged slopes in Lake Zurich (Switzerland)**	
2	Article Sub- Title		
3	Article Copyright - Year	**Springer-Verlag Berlin Heidelberg 2017 (This will be the copyright line in the final PDF)**	
4	Journal Name	Geo-Marine Letters	
5	Corresponding Author	Family Name	**Strupler**
6		Particle	
7		Given Name	**M.**
8		Suffix	
9		Organization	ETH Zurich
10		Division	Geological Institute
11		Address	Sonneggstrasse 5, Zurich 8092
12		e-mail	michael.strupler@erdw.ethz.ch
13	Author	Family Name	**Hilbe**
14		Particle	
15		Given Name	**M.**
16		Suffix	
17		Organization	University of Bern
18		Division	Institute of Geological Sciences and Oeschger Centre for Climate Change Research
19		Address	Bern
20		e-mail	
21	Author	Family Name	**Anselmetti**
22		Particle	
23		Given Name	**F. S.**
24		Suffix	
25		Organization	University of Bern
26		Division	Institute of Geological Sciences and Oeschger Centre for Climate Change Research
27		Address	Bern
28		e-mail	
29	Author	Family Name	**Kopf**

AUTHOR'S PROOF!

30		Particle	
31		Given Name	**A. J.**
32		Suffix	
33		Organization	MARUM – Center for Marine Environmental Sciences
34		Division	
35		Address	Bremen
36		e-mail	

37		Family Name	**Fleischmann**
38		Particle	
39		Given Name	**T.**
40		Suffix	
41	Author	Organization	MARUM – Center for Marine Environmental Sciences
42		Division	
43		Address	Bremen
44		e-mail	

45		Family Name	**Strasser**
46		Particle	
47		Given Name	**M.**
48		Suffix	
49		Organization	ETH Zurich
50	Author	Division	Geological Institute
51		Address	Sonneggstrasse 5, Zurich 8092
52		Organization	University of Innsbruck
53		Division	Institute of Geology
54		Address	Innsbruck
55		e-mail	

56		Received	20 September 2016
57	Schedule	Revised	
58		Accepted	2 January 2017

59 Abstract

Subaqueous landslides and their consequences, such as tsunamis, can cause serious damage to offshore infrastructure and coastal communities. Stability analyses of submerged slopes are therefore crucial, yet complex steps for hazard assessment, as many geotechnical and morphological factors need to be considered. Typically, deterministic models with data from a few sampling locations are used for the evaluation of slope stabilities, as high efforts are required to ensure high spatial data coverage. This study presents a simple but flexible approach for the probabilistic stability assessment of subaqueous slopes that takes into account the spatial variability of geotechnical data. The study area (~2 km^2) in Lake Zurich (northern Switzerland) shows three distinct subaquatic landslides with well-defined headscarps, translation areas (i.e. the zone where translational sliding occurred) and mass transport deposits. The ages of the landslides are known (~2,210 and ~640 cal. yr BP, and 1918 AD), and their triggers have been assigned to different mechanisms by previous studies. A combination of geophysical, geotechnical, and sedimentological methods served to analyse the subaquatic slope in great spatial detail: 3.5 kHz pinger seismic reflection data and a 300 kHz multibeam bathymetric dataset (1 m grid) were used for the detection of landslide features and for the layout of a coring and an in situ cone penetration testing campaign. The assignment of geotechnical data to lithological units enabled the construction of a sediment-mechanical stratigraphy that consists of four units, each with characteristic profiles of bulk density and shear strength. The thickness of each mechanical unit can be flexibly adapted to the local lithological unit thicknesses identified from sediment cores and seismic reflection profiles correlated to sediment cores. The sediment-mechanical stratigraphy was used as input for a Monte Carlo simulated limit-equilibrium model on an infinite slope for the assessment of the present slope stability and for a back analysis of past landslides in the study area, both for static and earthquake-triggered scenarios. The results show that the location of failure initiation in the model is consistent with stratigraphic analysis and failure-plane identification from sediment cores. Furthermore, today's sediment-charged slopes are failure-prone, even for a static case. This approach of including an adaptable sediment-mechanical stratigraphy into a limit-equilibrium slope stability analysis may be applied as well to the marine realm.

60	Keywords separated by ' - '	
61	Foot note information	The online version of this article (doi:10.1007/s00367-017-0492-8) contains supplementary material, which is available to authorized users.

Electronic supplementary material

ESM 1
(PDF 271 kb)

JrnlID 367_ArtID 492_Proof# 1 - 06/01/2017

Geo-Mar Lett
DOI 10.1007/s00367-017-0492-8

ORIGINAL

Probabilistic stability evaluation and seismic triggering scenarios of submerged slopes in Lake Zurich (Switzerland)

M. Strupler[1] · M. Hilbe[2] · F. S. Anselmetti[2] · A. J. Kopf[3] · T. Fleischmann[3] · M. Strasser[1,4]

Received: 20 September 2016 / Accepted: 2 January 2017

Abstract Subaqueous landslides and their consequences, such as tsunamis, can cause serious damage to offshore infrastructure and coastal communities. Stability analyses of submerged slopes are therefore crucial, yet complex steps for hazard assessment, as many geotechnical and morphological factors need to be considered. Typically, deterministic models with data from a few sampling locations are used for the evaluation of slope stabilities, as high efforts are required to ensure high spatial data coverage. This study presents a simple but flexible approach for the probabilistic stability assessment of subaqueous slopes that takes into account the spatial variability of geotechnical data. The study area (~2 km^2) in Lake Zurich (northern Switzerland) shows three distinct subaquatic landslides with well-defined headscarps, translation areas (i.e. the zone where translational sliding occurred) and mass transport deposits. The ages of the landslides are known (~2,210 and ~640 cal. yr BP, and 1918 AD), and their triggers have been assigned to different mechanisms by previous studies. A combination of geophysical, geotechnical, and sedimentological methods served to analyse the subaquatic slope in great spatial detail: 3.5 kHz pinger seismic reflection data and a 300 kHz multibeam bathymetric dataset (1 m grid) were used for the detection of landslide features and for the layout of a coring and an in situ cone penetration testing campaign. The assignment of geotechnical data to lithological units enabled the construction of a sediment-mechanical stratigraphy that consists of four units, each with characteristic profiles of bulk density and shear strength. The thickness of each mechanical unit can be flexibly adapted to the local lithological unit thicknesses identified from sediment cores and seismic reflection profiles correlated to sediment cores. The sediment-mechanical stratigraphy was used as input for a Monte Carlo simulated limit-equilibrium model on an infinite slope for the assessment of the present slope stability and for a back analysis of past landslides in the study area, both for static and earthquake-triggered scenarios. The results show that the location of failure initiation in the model is consistent with stratigraphic analysis and failure-plane identification from sediment cores. Furthermore, today's sediment-charged slopes are failure-prone, even for a static case. This approach of including an adaptable sediment-mechanical stratigraphy into a limit-equilibrium slope stability analysis may be applied as well to the marine realm.

Electronic supplementary material The online version of this article (doi:10.1007/s00367-017-0492-8) contains supplementary material, which is available to authorized users.

✉ M. Strupler
michael.strupler@erdw.ethz.ch

1 Geological Institute, ETH Zurich, Sonneggstrasse 5, 8092 Zurich, Switzerland

2 Institute of Geological Sciences and Oeschger Centre for Climate Change Research, University of Bern, Bern, Switzerland

3 MARUM – Center for Marine Environmental Sciences, Bremen, Germany

4 Institute of Geology, University of Innsbruck, Innsbruck, Austria

Introduction

Slope instabilities can have serious consequences in the marine and the lacustrine environment. As a consequence of unstable slopes, subaquatic landslides can occur, which in turn can produce tsunamis (Jiang and Leblond 1992). Both subaqueous landslides and landslide-triggered tsunamis can pose hazards to shore communities and to infrastructure onshore and at the sea/lake bottom (e.g. Prior et al. 1982; Tappin et al. 2001; Locat and Lee 2002; Schnellmann et al. 2002;

Masson et al. 2006; Dan et al. 2007). Stability evaluations of submerged slopes are thus crucial steps for assessing such hazards.

Various approaches for slope stability assessments (SSAs) exist, depending on the purpose and scale. Reflected in extensive documentation in the geotechnical literature, the limit-equilibrium method is used in most cases (Johari and Javadi 2012). With this method, a slope is considered unstable if the downward-driving shear stress exceeds the resisting shear strength (e.g. Kramer 1996; Abramson et al. 2002). Changes in stress and shear strength may result from various geological, physical and human-induced processes (e.g. erosion, rapid sedimentation, earthquakes, wave loading, water level changes and fluid escape; e.g. Locat and Lee 2002; Chapron et al. 2004). In many cases, the presence of a weak layer in the sedimentary succession facilitates slope failures (e.g. Craig 2004; Leynaud et al. 2004; Biscontin and Pestana 2006; Dan et al. 2007).

For earthquake-triggered landslides, back analyses are a valuable tool for estimating the intensities of past earthquakes (Leynaud et al. 2004; Strasser et al. 2007, 2011). The greatest uncertainties for SSAs are often associated with the soil properties (Craig 2004). Due to limitations in cost and time, slope stability models are often treated as deterministic models, considering data from a few sampling locations that are assumed to represent the characteristics of the entire slope. Hence, the spatial variability of slope geotechnical parameters often remains underexplored (Klaucke and Cochonat 1999; Leynaud and Sultan 2010). A probabilistic SSA is needed, however, to account for the spatial variation of the geotechnical properties and uncertainties (Chandler 1996; Lacasse and Nadim 1996; Leynaud and Sultan 2010; Johari and Javadi 2012). In many approaches, gradients of geotechnical parameters (e.g. density, shear strength) are used to estimate values with depth, providing acceptable results in areas where the thickness of lithological units shows little spatial variation (e.g. Strasser et al. 2011). However, the use of only a few gradients describing the geotechnical parameters within lithological units often ignores variations. Additionally, for locally very thick lithological units, extrapolation of data with gradients can lead to an overestimation of values.

The main aim of this study is to design a simple, powerful concept for a quantitative SSA under static and seismic loading that accounts for the spatial variability of geotechnical parameters. Compared to a deterministic analysis, a probabilistic analysis has the advantages of incorporating parameter uncertainty and allows the quantification of that uncertainty (Wolff 1996). A high spatiotemporal understanding of the slope characteristics is a prerequisite for constructing a probabilistic slope stability concept. This study focuses on a well-constrained slope in Lake Zurich, Switzerland, where three distinct subaquatic landslides with known ages have occurred (two of them interpreted as earthquake-triggered; Strasser and Anselmetti 2008; Strasser et al. 2013). High-resolution geophysical, geotechnical and sedimentological data from the undisturbed slope adjacent to the subaqueous landslides are used for a probabilistic SSA: Monte Carlo simulated (MCS) input data from a sediment-mechanical stratigraphy are integrated into a limit-equilibrium model. With this approach, the present study analyses (1) the location of failure initiation of the documented subaqueous landslides, (2) the pseudostatic critical acceleration needed to create the two earthquake-triggered landslides in the study area and (3) the current slope stability with the present sediment drape under static and possible earthquake-shaking conditions.

Physical setting and previous studies

Lake Zurich is a glacially overdeepened, perialpine lake in northern Switzerland (~47°N, 8.5°E, 406 m a.s.l.), which consists of Lake Zurich sensu stricto and the upstream Obersee (Fig. 1). The two parts of the lake are separated by an end moraine from the last glaciation. Within Lake Zurich, an escarpment in the molasse bedrock separates an up to 136 m deep northern basin with steep slopes and a flat basin plain from a ~25 m deep southern basin (Schindler 1974). The molasse bedrock is overlain by an up to ~154 m thick Quaternary infill, consisting of glacial, glaciolacustrine and lacustrine deposits (Schlüchter 1984; Lister et al. 1984). The permeability of the molasse bedrock in the study area has been described as very low (Bitterli et al. 2004).

The postglacial sedimentary succession in the deep basin (Table 1) is known from previous studies (Schindler 1974; Gyger et al. 1976; Giovanoli 1979; Strasser and Anselmetti 2008): The till-covered bedrock is overlain by a thick succession of late glacial bluish to light grey muds (with high plasticity), which originate from current-dispersed suspended sediment (Schindler 1974). The lower part of these plastic muds contains some ice-rafted debris, which disappear in the upper part (Gyger et al. 1976). The latter shows some cm-thick lamination, interpreted as produced by glacial cycles by Giovanoli (1979). The overlying sediments display a beige colour, which indicates aeolian input of sediment exposed to surface weathering (Giovanoli 1979). During the Younger Dryas, blackish iron sulphide muds, containing small organic particles and almost no carbonate, were deposited. With subsequent further warming into the Holocene, lacustrine chalks and marls were deposited (Schindler 1974; Gyger et al. 1976; Giovanoli 1979). In contrast to this basinal sequence, the sedimentary succession on the slopes has not been systematically analysed so far. Moreover, no publically available high-resolution geotechnical survey data exist for the slopes of Lake Zurich. Only some data on the mechanical behaviour of the postglacial sediments in the southern part of Lake Zurich are available (Gyger et al. 1976), where it was

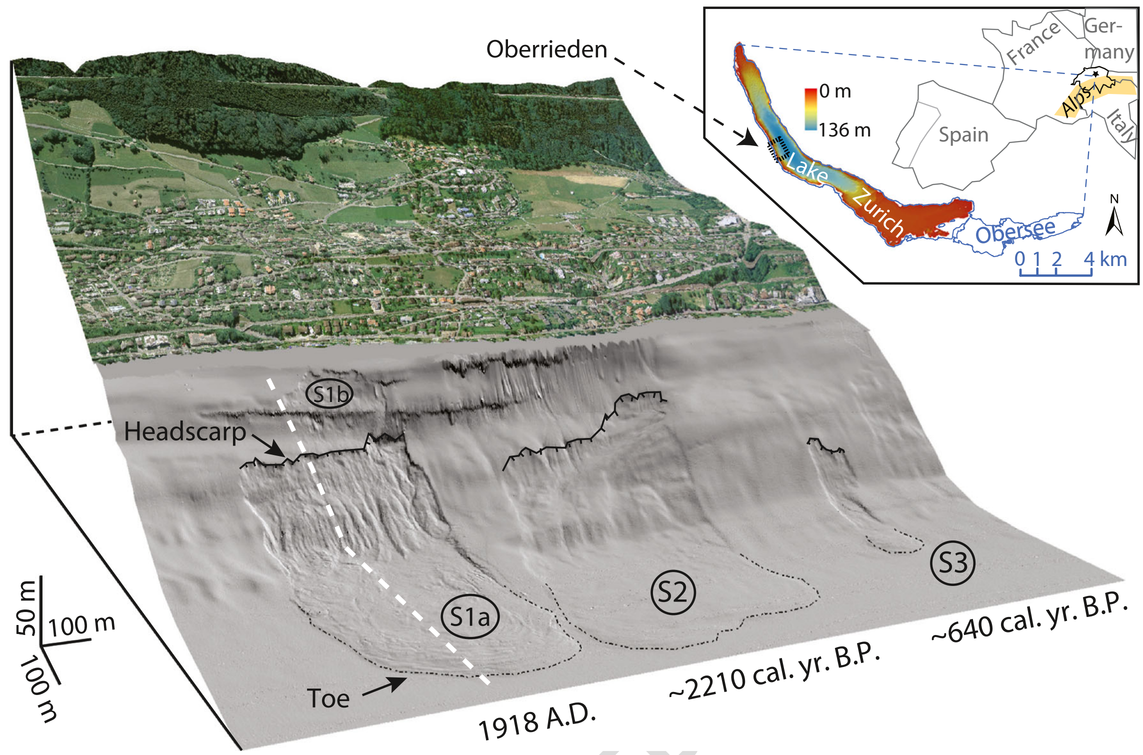

Fig. 1 Three-dimensional representation of the DDM representing the study area. The southernmost landslide (S1a) occurred in 1918 AD, the slide in the centre (S2) ~2,210 cal. yr BP, and the slide in the north (S3) ~640 cal. yr BP. Vertical exaggeration: 3×. View towards the west. *Dashed white line* Seismic profile shown in Fig. 2. Subaqueous DDM: Strupler et al. (2015). Subaerial LiDAR-DEM and Orthophoto: Swisstopo

concluded that the physical characteristics of the different lithological units vary strikingly. A study by Strasser et al. (2008) classified the postglacial lithological succession in three lithological units (LUs) and dated them (Table 1). The present study refers to that classification.

Since deglaciation, subaquatic mass movements occurred repeatedly in Lake Zurich's deep basin, triggered by sediment overload, earthquakes or anthropogenic influence on the shores (Schindler 1976; Kelts and Hsü 1980; Strasser et al. 2006, 2013). Strasser and Anselmetti (2008) provide well-constrained ages for the landslides. For five events with simultaneously triggered subaquatic mass movements, earthquakes are the assumed trigger (Strasser and Anselmetti 2008). Synchronous basinwide landslide occurrences are a typical signature for earthquake-triggered landslides in perialpine lakes (e.g. Schnellmann et al. 2006; Strasser et al. 2013). In the last ~150 years, a few subaquatic landslides have occurred in the northern basin of Lake Zurich, all triggered by human activity (e.g. Heim 1876; Nipkow 1927; Kelts and Hsü 1980).

Table 1 Postglacial lithological units and their ages (Strasser et al. 2008)

Lithological unit	Age
LU3b: lacustrine marls	Present day to ~7,000 cal. yr BP
LU3a: lacustrine chalks	~7,000 to ~12,000 cal. yr BP
LU2: iron sulphide muds	~12,000 to ~14,500 cal. yr BP
LU1: late glacial plastic muds	~14,500 to ~17,600 cal. yr BP

The study site is located on the western flank of the northern basin, offshore the village of Oberrieden. In an area of ~2 km^2, the site comprises three distinct NE-facing translational, frontally confined subaquatic landslides (Fig. 1). The southernmost landslide (S1a in Fig. 1 and Table 2), dated to 1918 AD, was triggered by human activity onshore (Nipkow 1927). The slides in the middle sector (S2 in Fig. 1 and Table 2, ~2,210 cal. yr BP) and in the north (S3 in Fig. 1 and Table 2, ~640 cal. yr BP) are assumed to have been triggered by earthquakes (Strasser and Anselmetti 2008). Because the slope is not affected by river inflows and shows no fluid-escape features in the bathymetric dataset, and because the bedrock has a very low permeability, the site is well suited for a simple SSA approach.

Upslope of S1a, in the shallow nearshore area (~10 m water depth; Fig. 1), a smaller eroded patch (S1b) with a ~4 m high headscarp and an areal coverage of ~15,000 m^2 can be found. No visible connection occurs between the main slide S1a and S1b. However, a part of the eroded material of the small, upper slide is deposited directly above the headscarp of S1a (Fig. 1). Between the extents of each slide, some patches of undisturbed sediment drape exist. The two slides S1a and S2 show similar outlines and dimensions and their eroded sediment

Table 2 Overview characteristics of the slides (Strupler et al. 2015)

	S1a	S2	S3
Age	1918 AD	~2,210 cal. yr BP	~640 cal. yr BP
Erosion area (m^2)	~160,000	~150,000	~17,000
Depth headscarp (m below lake level)	51	42	76
Max. water depth of deposits (m below lake level)	135	135	133
Runout distance (m)	865	791	383
Height of headscarp (m)	~5	~5–7	~3–4
Landslide volume (m^3)[a]	~800,000	~750,000 to 1,050,000	~51,000 to 68,000

[a] Estimated by multiplication of erosion area and headscarp height

volume is estimated at about 10^6 m^3 (Table 2). Their failure scars extend laterally to ~400 m.

Reflection seismic data from the slopes (Strasser and Anselmetti 2008) display a seismic-stratigraphic unit with continuous parallel reflections of alternating amplitudes that overlies a unit with a chaotic, high-amplitude facies, which, in turn, covers the acoustic basement. Figure 2 shows a seismic reflection profile along S1a (cf. dashed white line in Fig. 1), revealing an irregular slope with an alternating gradient (Fig. 2a). Between ~40 and 70 ms TWT, a steep zone (>30°) can be identified where no significant sedimentation occurs. A closeup of the failure scar of S1a (~5 m high; Table 2) can be found in Fig. 2b. The area affected by mass transport deposits (MTDs), characterized by a typical chaotic-to-transparent seismic facies (e.g. Schnellmann et al. 2002; Strasser and Anselmetti 2008), is highlighted in blue. It shows deformation of the basin-plain sediment ('frontal thrusting') expressed by topographic bulges (e.g. Schnellmann et al. 2005).

A short gravity core taken by Strasser et al. (2013) revealed that the glide plane of S1a consists of glacial deposits. This finding raises the question of whether the glide plane is located in the same lithological unit (or even in a specific weak layer within a unit) for all other subaqueous landslides in the study area and throughout each respective slide. A back analysis of the subaqueous landslides may support the seismic triggering with geotechnical arguments and quantitatively constrain pseudostatic critical accelerations needed to cause failure of these known occurrences.

Materials and methods

Geophysical data acquisition

A survey with a Kongsberg EM2040 multibeam echosounder (300 kHz) yielded a new high-resolution (1 m grid) digital depth model (DDM) of Lake Zurich (Strupler et al. 2015), enabling the investigation of the extent and geomorphic features of subaqueous landslides (Fig. 1). Slope gradient values derived from the DDM with a geographic information system (GIS) were used as input for the slope stability model. Calculations were done at a 5 m grid resolution.

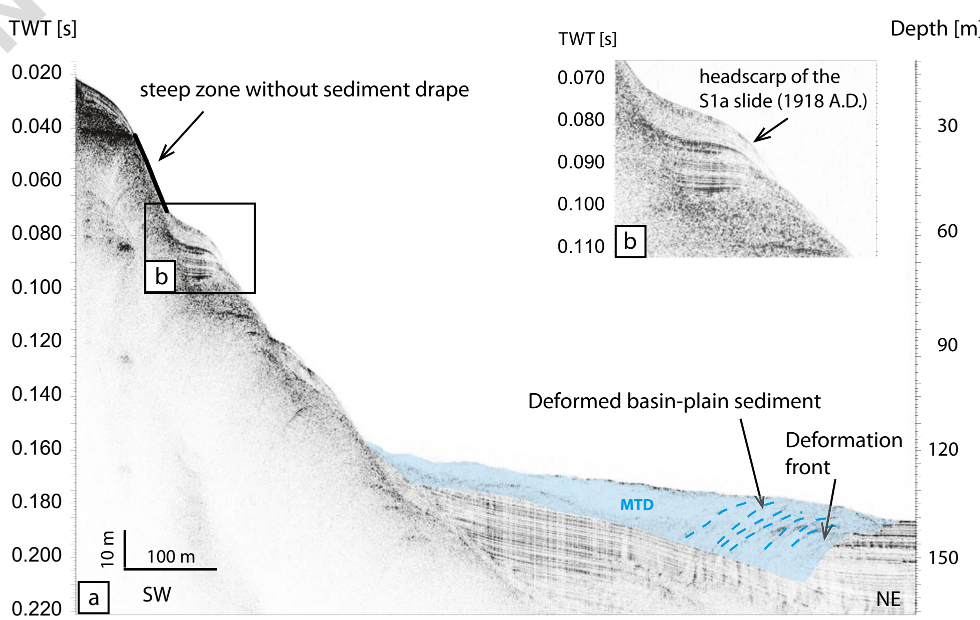

Fig. 2 Seismic profile of S1a (modified after Strasser und Anselmetti 2008). Seismic data are unmigrated, so that true geometries and sharp edges are masked by diffractions. Location of profile is shown on Fig. 1

An existing 3.5 kHz pinger seismic dataset (Strasser and Anselmetti 2008) was complemented by additional 3.5 kHz seismic data acquired in 2016 with the same equipment. No migration was applied to the seismic data. Conversion from two-way travel time to depth was conducted assuming a sonic velocity of 1,500 m/s. The DDM and seismic dataset were used to determine locations for sediment coring and in situ cone penetration testing (CPT; Fig. 3).

Sediment coring and laboratory analysis

On the slopes offshore Oberrieden, seven Kullenberg-type piston cores (2.8 to 6 m long; Kelts et al. 1986) and 21 short gravity cores (maximum length: 1.3 m) were recovered from the floating platform ARARAT and from the research vessel ArETHuse respectively (Fig. 3). A handheld GPS device was used for positioning. The Kullenberg-type cores (except for ZH15-K13, which was taken in the translation area) were collected from the undisturbed slope sediments adjacent to the landslides to recover a continuous sedimentation record (Fig. 3). The short sediment cores were taken in the translation area to investigate the glide plane.

A sedimentological and geotechnical characterization of the cores was conducted in the laboratory. Bulk density ρ_{bulk} and magnetic susceptibility of the sediment core were logged with a multi-sensor core logger (MSCL; Geotek, Daventry, UK) using a sample interval of 1 cm. Subsequently, the sediment cores were split in two halves, photographed, and macroscopically described. Water content was measured by drying samples (sampling interval ~50 cm) in an oven for 24 h at 110 °C, following Blum (1997). Grain-size distribution was measured with a Malvern Mastersizer 2000s for selected cores (sampling interval ~50 cm). The undrained shear strength (s_u) was measured with a cone penetrometer at intervals of 5 cm. In addition, s_u was measured with laboratory vane tests at intervals of 50 cm.

CPT probing

In situ s_u profiles were measured using a free-fall CPT probe from Marum, Bremen (Stegmann et al. 2006a, 2006b) deployed from the ARARAT platform. The apparatus derives s_u from the measured resistance of the cone and the sleeve of the probe (Stegmann et al. 2006b). Configuration of the CPT length was adapted to thicknesses of seismic stratigraphic units, and varied between 2 and 6 m. For a more detailed information on CPT testing and processing, refer to Steiner et al. (2012) and Steiner (2013). Processing was conducted using a Nk value of 16. To cancel noise in the CPT s_u data, a 50 pt moving window filter was applied.

Slope stability assessment

SSA was conducted with a limit-equilibrium model on an infinite slope for a static case and for earthquake-triggered scenarios. The infinite-slope model assumes planar slopes of infinite extent with a slope-parallel failure surface. Also, the failure depth is small compared to the length of the slope (Craig 2004; Coduto et al. 2011). An SSA was conducted along three transects on undisturbed sediment patches between the subaqueous slides. Each transect was analysed for reconstructed sediment drape thicknesses at the time of the S2 and S3 slides (with a sedimentation model; see Results section), and of the present-day conditions. The slope conditions (e.g. the slope gradient and thickness distribution of lithological units) are assumed to be similar to those in the neighbouring failed areas.

Water-saturated sediments with a low hydraulic conductivity are often assumed to be under undrained conditions when subjected to fast load changes, since water cannot flow into or out of the soil in a short time (Coduto et al. 2011). Therefore, the shear strength of Lake Zurich's slope sediments is described by s_u. The s_u data measured in situ by CPT were considered for the SSA. In a first step, the geotechnical data for ρ_{bulk} and s_u were assigned to lithological units, based on patterns of geotechnical parameters and visual core description. With these geotechnical

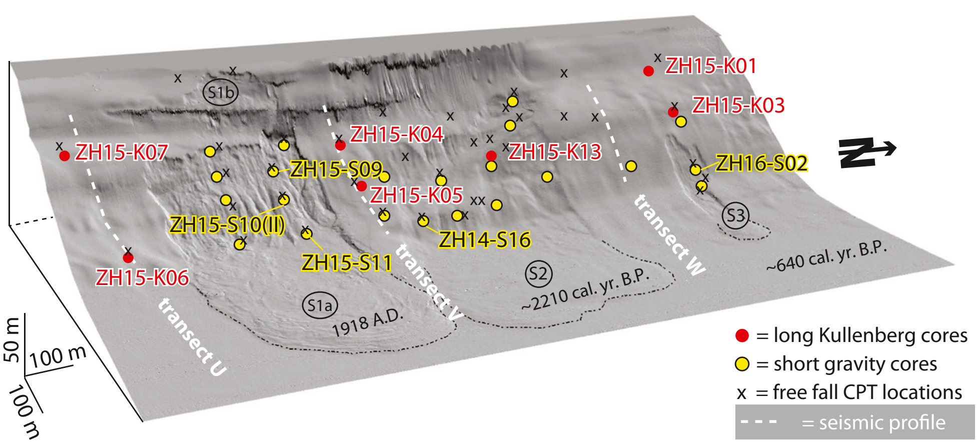

Fig. 3 Three-dimensional illustration of the study area with sediment core (*red* Kullenberg-type cores, *yellow* short gravity cores) and CPT locations. Vertical exaggeration: 3×. View towards the west. For coordinates, water depths and slope gradients of the core and CPT locations, refer to electronic supplementary material (Tables ESM1 and ESM2)

data coupled to lithological units, a sediment-mechanical stratigraphy was constructed (see Results section).

The factor of safety (FS) on an infinite slope under undrained conditions was calculated according to Eq. 1 (Coduto et al. 2011):

$$FS = \frac{s_{u^\circ}}{\gamma' * D * \sin\alpha * \cos\alpha} \quad (1)$$

where γ' is the submerged unit weight, D the vertical depth below the lake bottom and α the slope gradient. Pore pressure is not considered in the equation, as the undrained shear strength is used.

A Matlab (Mathworks, Inc.) routine was used to calculate a deterministic FS-depth profile, the probability of failure (PoF) as well as the critical pseudostatic acceleration (a_c) needed to cause failure at selected model locations. The model conducts an independent SSA for each model location, assuming that each location is on an infinite slope with its respective slope gradient. The deterministic FS was calculated using the mean ρ_{bulk} and s_u from in situ CPT for each depth step from the sediment-mechanical stratigraphy.

For the probabilistic SSA in an MCS, 2,500 FS-depth profiles were calculated for each model location with randomly sampled data from lognormal ρ_{bulk} and s_u distributions for each depth step. A lognormal distribution was used to avoid negative input values (e.g. Tobutt 1981; Lacasse and Nadim 1996; Abramson et al. 2002). The PoF results from the percentage of values in the FS distribution less than 1 (Chandler 1996).

The vertical error of the bathymetry (~0.5 m; Strupler et al. 2015) was simulated (MCS) in GIS after Zandbergen (2011) by adding a spatially auto-correlated error term to the original DDM. Subsequently, 2,500 simulated slope maps were derived and implemented in the Matlab code.

a_c represents the effect of an earthquake by adding a constant acceleration to the failure mass (e.g. Kramer 1996). Therefore, it provides only approximate information on earthquake shaking (Jibson 2012). a_c, calculated with Eq. 2, assumes that the seismic force acts parallel to the slope (Newmark 1965; Jibson 1993):

$$a_c = (FS - 1) * g * \sin\alpha \quad (2)$$

To assess the quality of the results from the model, 2D profiles of the undisturbed slope with geotechnical data were used as an input for the professional SSA software SLIDE (Rocscience, Inc.). SLIDE conducts a 2D limit-equilibrium SSA to calculate a global mean FS with the Morgenstern and Price (1967) method.

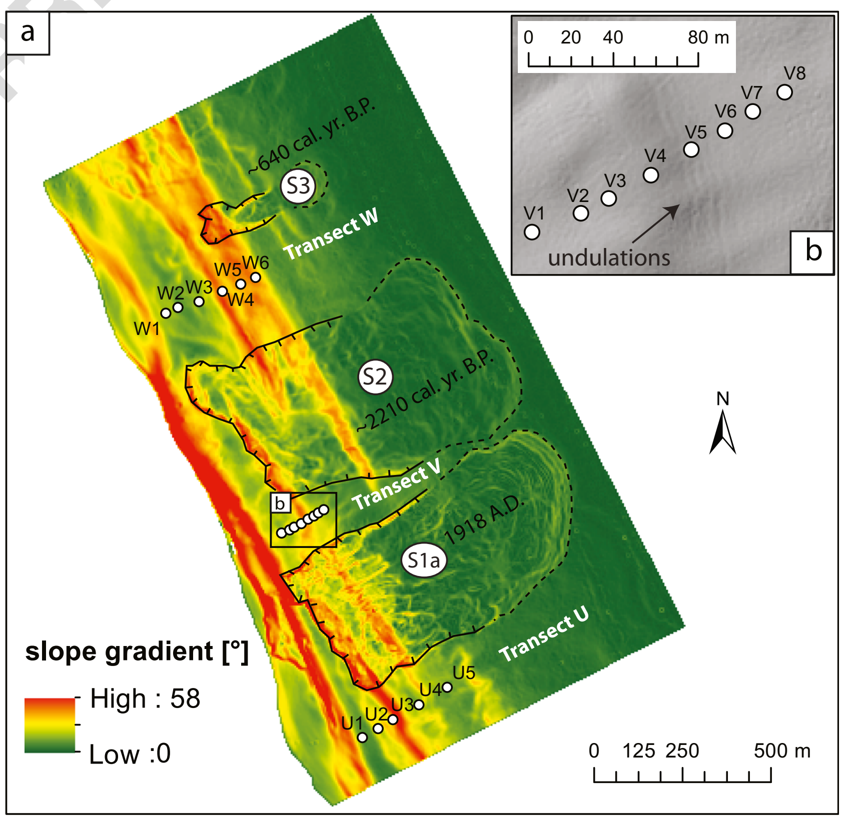

Fig. 4 **a** Slope gradient map and location of transects for modelling slope stability. **b** Slope-transversal undulations on a shaded relief map

Results

Slope characteristics

Geomorphic characteristics of the study area

Slope gradients vary between 0° and 58°, comprising alternating flat terraces (~5–10°) and steeper zones (~10–20°; Figs. 2 and 4a). The headscarps of the three subaqueous slides are situated in the upper part of a steep zone (S1a and S2) or within a steep zone (S3). In the unfailed sediment patch between S1a and S2 (Fig. 1), a series of linear, isobath-parallel undulations with a width of ~5 m and an amplitude of ~10 cm can be identified in the shaded relief (~80–90 m water depth, ~20° slope gradient; Fig. 4b). These undulations cannot be identified in the reflection seismic dataset because the lateral dimension of the features is slightly lower than the lateral resolution (footprint) of the 3.5 kHz pinger seismic data at that depth.

Lithological units of the undisturbed slope

The six Kullenberg cores taken on the undisturbed slope (Fig. 3) enable a characterisation of the lithological succession on the slope. Core description and changes of geotechnical patterns allow the definition of different lithological units and subunits (Fig. 5; cf. Figs. 6 and 7), labelled in agreement with the postglacial lithological succession in Lake Zurich (Strasser et al. 2008). Depending on the water depth and slope gradient at the core locations, the individual unit thicknesses per core vary.

Describing from top to bottom, LU3c has a thickness of 10–60 cm and shows alternating organic and calcite couplets that represent varves, originating from lake eutrophication after the end of the 19th century (e.g. Kelts 1978; Giovanoli 1979). Due to the applied coring method, LU3c could not be recovered completely for some cores. Thickness of LU3c for those cores was estimated from neighbouring short cores. LU3b (1.1–3 m thick) consists of dark-brown Holocene marls with a high silt content (~75–85%) and high water contents (more than 100% of dry weight). LU3a (0.7–1.4 m thick) shows a beige-white colour, a high sand content (up to 30%) and a high carbonate content. LU2 (0.15–0.5 m thick) is characterized by dark-grey to black clayey silts and low ρ_{bulk}. LU1 consists of a generally thin, beige-grey, homogeneous uppermost part with a strongly variable thickness amongst the cores (labelled as LU1b/c; subunits b and c described in Strasser et al. 2008 for the deep basin cannot be distinguished on the slopes). A bluish-grey, laminated part with densities of ~1.6 g/cm^3 (thickness: 0.1–2.9 m) in the middle (labelled as LU1a) can be distinguished from a lower part with dropstones. The occurrence of the dropstones is associated with an increase of ρ_{bulk} to >1.8 g/cm^3. LU1 is rich in clays (>25% clay content). Underneath the late glacial sediments of LU1, till occurs (Giovanoli 1979). Typically, the till shows poor sorting, no stratification, and the clasts are mostly angular (core ZH15-K13 in Fig. 6b) with ρ_{bulk} >2 g/cm^3.

Mechanical properties of the undisturbed slope

In all cores, the profiles of the sediment physical properties show characteristic patterns that generally correlate with the lithological units. Profiles of ρ_{bulk} and s_u show distinct changes at the boundaries between LU3b and LU3a, as well as at the boundaries between LU3a and LU2, between LU2 and LU1, and between the upper part of LU1 without clasts and the lower part with clasts (Fig. 5).

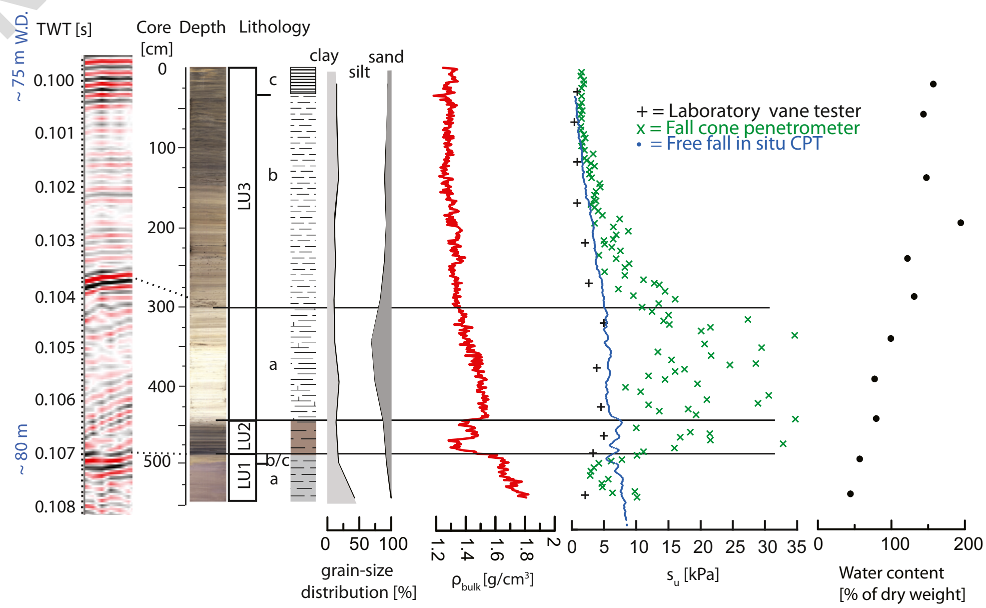

Fig. 5 Sediment-mechanical properties of the undisturbed slope, here at location ZH15-K04 (refer to Fig. 3 for core location)

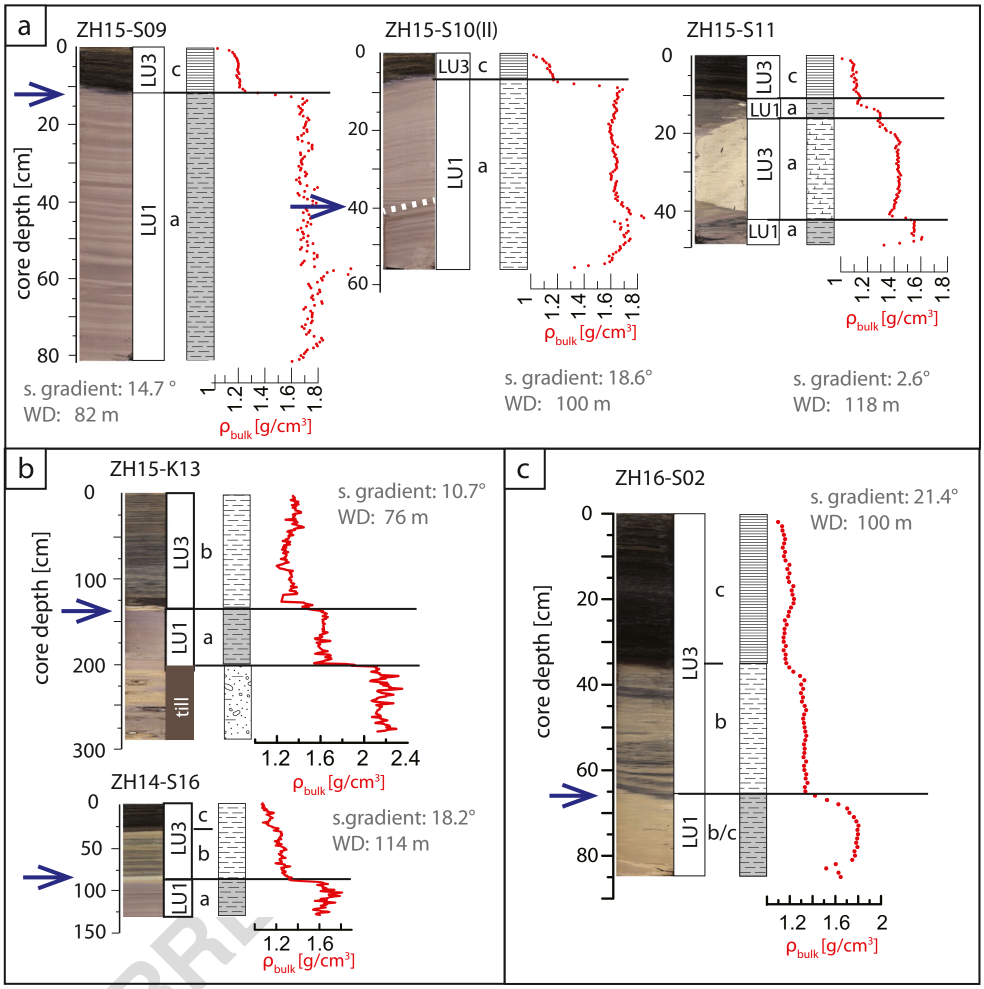

Fig. 6 Characteristics derived from sediment cores in the translation area of the three subaqueous landslides. **a** Short cores taken on a transect in the translation area of the S1a slide. *Dashed white line* Sharp change in lamination angles. **b** Cores taken in the translation area of S2. **c** Short core taken in the translation area of S3. *Blue arrows* Glide plane, *S. gradient* slope gradient, *WD* water depth. Refer to Fig. 3 for core locations

ρ_{bulk} data show a slight linear increase with depth in LU3c and LU3b. In LU3a, the ρ_{bulk} profile has a convex shape that increases with depth to values of ~1.5 g/cm^3. It drops to a value of ~1.3 g/cm^3 in LU2 before it strongly increases to values exceeding 1.6 g/cm^3 in LU1.

The absolute values of s_u derived from different methods in situ and in the laboratory differ: results from the laboratory vane tests show the lowest values whereas the fall-cone tests show the highest values. In general, the three methods show a similar pattern: an increase of s_u with depth in the uppermost LU3b, roughly constant values in LU3a, fluctuations in LU2, and a decrease in values between LU2 and LU1. The s_u values measured with the fall cone are significantly higher for LU3a and LU2 when compared to LU1 and LU3b.

Generally, water content decreases linearly with depth. LU3c and U3b have water contents between 194 and 122% of dry weight (mean: 148%), LU3a between 74 and 136% of dry weight (mean: 99%), LU2 between 88 and 168% (mean: 128%), and LU1 between 46 and 73% (mean: 56%).

Core-to-seismic correlation

The uppermost seismic stratigraphic unit with a facies of continuous parallel reflections is separated by two strong positive amplitude reflections. These reflections can be assigned from core-to-seismic correlation to the transition of LU1 to LU2 (slight increase in ρ_{bulk} and thus acoustic impedance) and the transition of LU3a to LU3b (distinct increase in ρ_{bulk}/impedance; Figs. 5 and 8). The transition between LU2 and LU3a cannot be differentiated with the reflection seismic data. The chaotic high-amplitude facies can be assigned to the till, and the acoustic basement to the molasse bedrock or till (distinction not always possible).

Lithological characteristics of the translation area

Results from the sediment cores taken in the translation areas of the subaquatic landslides show that Holocene marls (LU3b) and varves (LU3c) directly overlie late glacial plastic muds (LU1), and that LU3a and a large part of LU3b are missing (Fig. 6). These unconformities are also expressed in a sharp increase of ρ_{bulk} to ~1.6 g/cm^3.

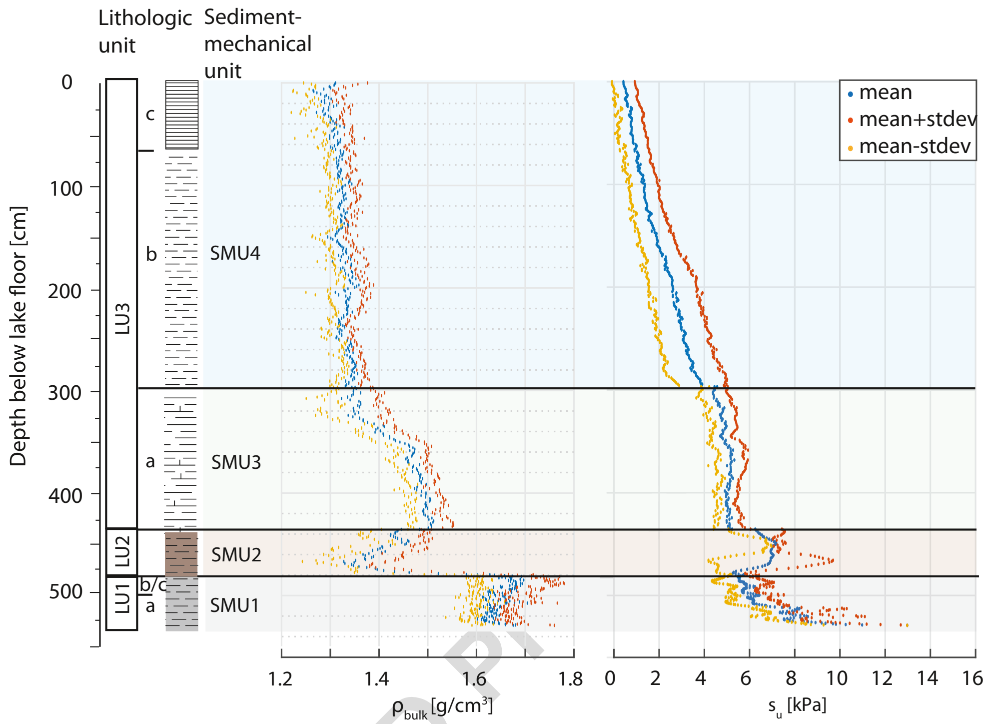

Fig. 7 Sediment-mechanical stratigraphy, showing mean ρ_{bulk} and mean s_u values from multiple Kullenberg-type cores and CPT locations respectively (*blue*). *Yellow dots* Mean values minus one standard deviation, *red dots* mean values plus one standard deviation. With this input, probability-density functions can be made for each depth step, and be used to select random values for each MCS run (here: mechanical units stretched to thicknesses of the lithological units at location K04)

Figure 6a shows three short cores taken along a depth transect of the slope eroded by S1a. In all three cores, a ~10 cm thick LU3c covers directly LU1a. For the topmost core in the transect (ZH15-S09), LU1a shows an undisturbed succession, whereas for the cores located more downslope (ZH15-S10(II) and ZH15-S11) LU1a is disturbed. Core ZH15-K13 from the translation area of S2 shows that most of LU1 has been eroded by the subaqueous landslide, as only ~70 cm of LU1a cover the underlying till (Fig. 6b). Core ZH14-S16, recovered near the toe of the slope, reveals the same stratigraphic depth of the glide plane. Thicknesses of LU3b and LU3c vary between 90 and 135 cm (see electronic supplementary material Table ESM3), depending on the water depth and slope gradient of the respective coring location. The core photograph and ρ_{bulk} profile of short core ZH16-S02 in the translation area of S3 (Fig. 6c) show that LU3b covers LU1b/c. Erosion of S3 does not reach as deep as for S1a and S2, where LU1b/c is missing in the cores in the translation areas.

Sediment-mechanical stratigraphy

The observation that s_u values from in situ CPT, laboratory fall-cone and vane-shear tests vary may be due to (1) s_u being significantly anisotropic (e.g. Craig 2004) or (2) different working concepts and calibration of the measuring devices. This study considers the s_u values from in situ CPT for the SSA, as the many data points obtained with this method qualify for statistical analysis (Lacasse and Nadim 1996). Furthermore, in situ CPT testing can be better than laboratory methods for assessing the engineering properties of calcareous soils (such as lacustrine chalks; LU3a), due to difficulties in obtaining undisturbed samples for laboratory testing (Lunne et al. 2002).

The present study synthesizes a mechanical stratigraphy based on the fact that the profiles for ρ_{bulk} and CPT-derived s_u of each sediment core's lithological units show a similar pattern but different thicknesses, due to different sedimentation at the different coring locations (electronic supplementary material Table ESM5). The geotechnical profiles per lithological unit amongst the sediment cores are stretched to a standard unit length (Eq. 3). By combining the geotechnical data per normalized unit from all the cores, the mean ρ_{bulk} and s_u profiles and their standard deviation per unit are calculated. For model simplicity reasons, stress history is neglected:

$$z_{\text{normalized}(i)} = \frac{z(i) - \min.(z(i))}{\text{length}(z(i))} * 100\,\text{cm} \qquad (3)$$

where $z(i)$ is the depth vector of lithological unit i (cm) and $z_{\text{normalized}(i)}$ is the normalized length of unit i (cm).

The *sediment-mechanical stratigraphy*, consisting of four distinct sediment-mechanical units (SMUs), includes the spatial variability of the ρ_{bulk} and s_u data (Fig. 7). *SMU1* starts at the top of LU1 and ends where dropstones occur in the lower part of LU1a. Throughout the whole SMU1, density is greater than 1.6 g/cm^3. In situ s_u values from CPT increase from ~5 kPa at the unit top to ~10 kPa at the unit bottom.

SMU2 is defined as the part of the geotechnical profile containing LU2. Here, the ρ_{bulk} decreases sharply from ~1.5 to 1.35 g/cm^3 and the CPT s_u values fluctuate strongly.

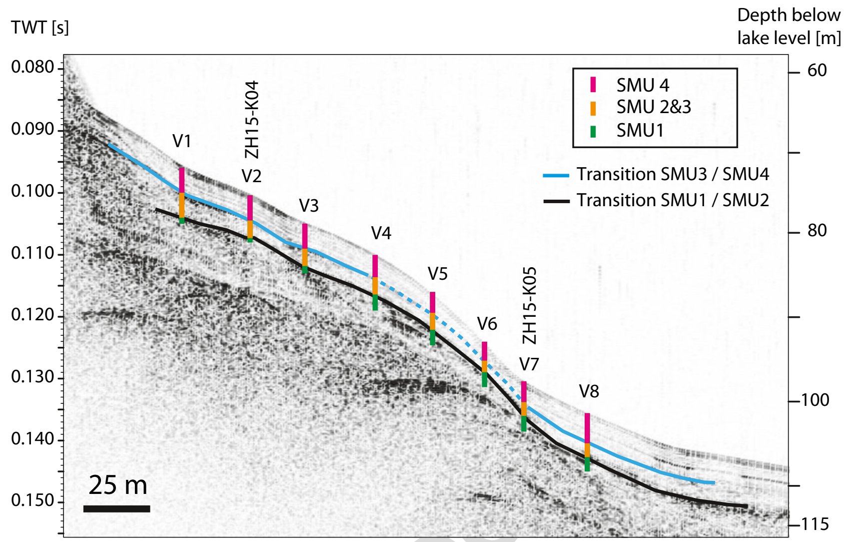

Fig. 8 Thicknesses of sediment-mechanical units according to core-to-seismic correlation. *Black and blue horizons* Strong reflections between SMU1 and 2 as well as SMU3 and 4 respectively. The dashed part of the blue horizon is interpreted, as the reflection was not visible in that part of the profile. Thicknesses of the individual units at the selected model locations V1–V8 can be found in the electronic supplementary material (Table ESM10). See Figs. 3 and 4 for locations of transects. Seismic profile modified after Strasser and Anselmetti (2008)

SMU3 is defined by a convex shape in the ρ_{bulk} profile, which increases with depth from values of ~1.35 to ~1.5 g/cm^3, and by the constant s_u values of in situ CPT data (~5 kPa). SMU3 corresponds to LU3a.

SMU4 starts at the sediment surface and ends at the boundary between LU3b and LU3a. ρ_{bulk} at the unit top is ~1.3 g/cm^3 and increases linearly to ~1.35 g/cm^3 at the unit bottom. s_u increases downcore linearly

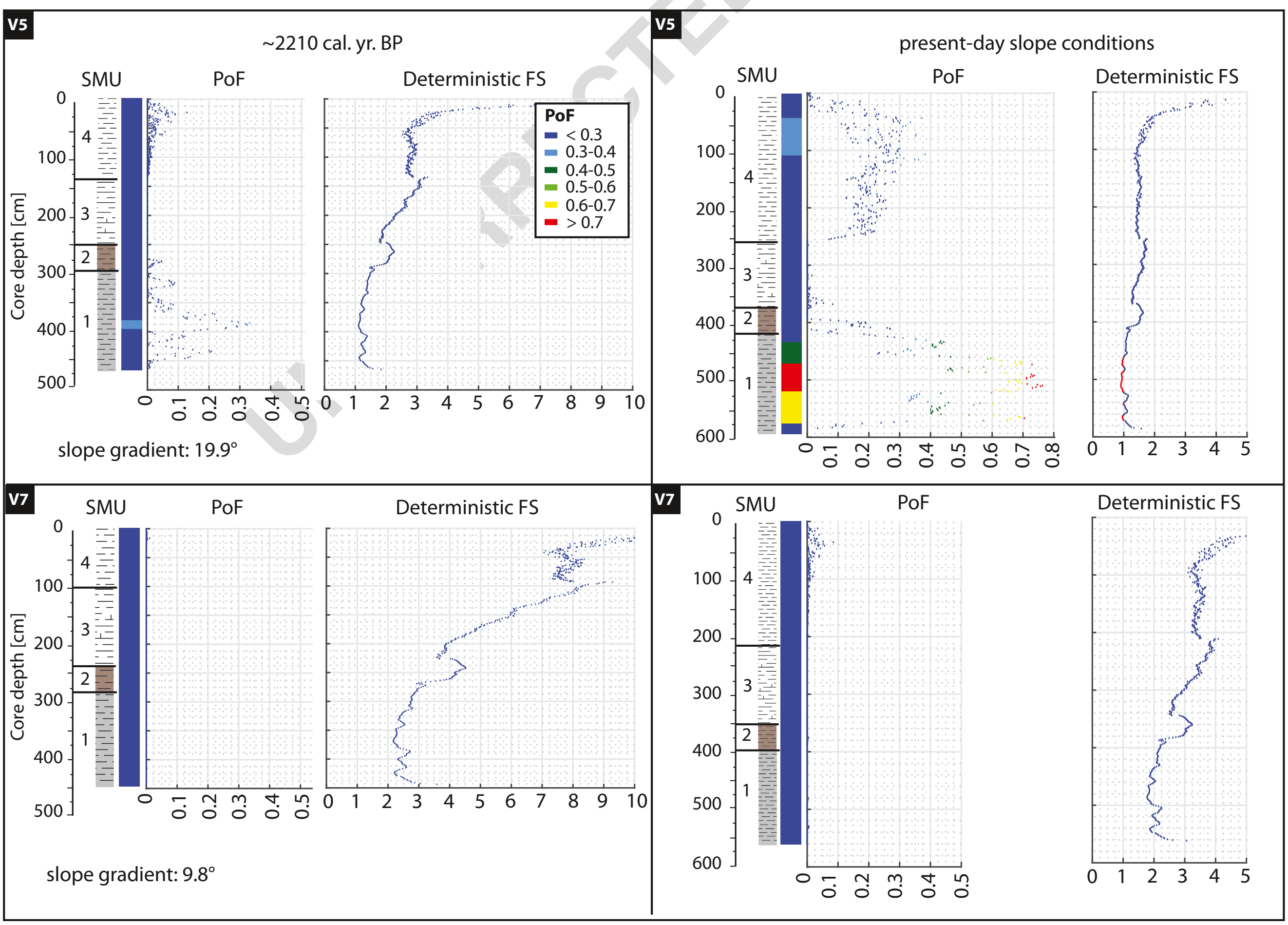

Fig. 9 PoF and deterministic FS for the back-calculated sedimentary drape ~2,210 cal. yr BP (*left*) and for the present-day sedimentary drape at locations V5 (*top*) and V7 (*bottom*)

from ~1 kPa at the top of the unit to ~4 kPa at the bottom.

While the amount of geotechnical input data for the mean ρ_{bulk} profile remains constant (n=6 cores) throughout the sediment-mechanical units (as ρ_{bulk} was measured in the laboratory on the cores), the amount of in situ CPT s_u profiles varies within the sediment-mechanical units, due to different penetration depths of the CPT device (n=8 for SMU4, n=6 for SMU3, n=4 for SMU2 and SMU1). The variability of the geotechnical data can be described by the coefficient of variation (CV, i.e. standard deviation divided by mean of a dataset). The CV of the ρ_{bulk} data is much smaller than that of the in situ CPT data (electronic supplementary material Table ESM6). The highest variability in CPT s_u values is found in SMU4 (CV ~0.5) and the lowest variability in SMU3 (CV ~0.1).

Sedimentation model

From all the short cores taken in the translation areas, the thickness of the undisturbed sediment drape covering the glide plane (Fig. 6 and electronic supplementary material Table ESM3) can be related to the slide age and water depth. A multivariate linear regression (electronic supplementary material Table ESM4) leads to an empirical equation for estimating the sedimentary drape accumulation on the slope as a function of age and water depth (Eq. 4)—sediment drape accumulation (ΔZ, cm) since a landslide occurred at any location p:

$$\Delta Z_p(w,t) = 0.046{*}t_p - 0.31{*}w_p + 44.476 \qquad (4)$$

where t_p is the age of landslide at location p (years) and w_p the water depth (m).

The reason for choosing this purely empirical model instead of one based on reconstructed sedimentation rates (dependent on water depth and slope gradient) is that the latter performs poorly. The presented linear regression provides good results for this particular slope for the thickness of the Holocene marls but should not be considered as valid for the whole basin.

Adapting sediment-mechanical units to local conditions

Using the core-to-seismic correlation, the thicknesses of SMU4 as well as the combined thickness of SMU2 and SMU3 can be calculated for any location where a reflection seismic profile exists. The thickness of SMU2 in the sediment cores of the present study is much smaller than the thickness of SMU3. With data from neighbouring sediment cores, the thickness of SMU2 is estimated and subtracted from the combined thickness of SMU3 and SMU2 to estimate the thickness of SMU3. The thickness of SMU1 can also be estimated from neighbouring cores.

Slope stabilities

Static slope stability assessment

Thicknesses to subtract from the sediment drape for the model locations at the time of the S2 and S3 slides can be found in the electronic supplementary material (Table ESM11). Within the transects U, V and W, stabilities of the single modelled locations vary strongly (Figs. 9 and 10). Figure 9 shows PoF-depth and deterministic FS-depth profiles for a static scenario at two selected locations V5 and V7, both for the present situation and for the situation at the time of S2.

As the FS is directly proportional to s_u, a change in s_u with depth has a strong impact on the FS-depth profile. FS is also inversely proportional to the bulk density, slope gradient and thickness of the sediment drape covering the potential glide plane. This is demonstrated at the locations V5 and V7 (Figs. 9 and 10), which have similar SMU thicknesses: at V5, a slope gradient that is about twice as steep (~20° vs. ~10°) causes a decrease of the FS by a factor of 2 (minimum FS 1.1 vs. 2.2 for the FS-depth profiles of S2 and 0.9 vs. 1.8 for the present-day scenario). Generally, in the FS-depth profile, the FS decreases with depth. In SMU4, it decreases hyperbolically, in SMU3 linearly, and in SMU2 the FS increases again before decreasing smoothly in SMU1. Performing a back analysis of S2, i.e. reducing the sedimentary drape from the present-day situation by 122 cm (V5) and 119 cm (V7), increases the minimum FS of the FS-depth profiles towards a more stable situation by 0.2 for V5 and by 0.4 for V7.

Most of the PoF-depth profiles show PoF >0 in the uppermost part of SMU4, although the deterministic FS are much greater than 1 (Fig. 9). A high FS does not necessarily correspond to a low PoF (Nadim et al. 2005) as their relationship depends also on the uncertainties of the geotechnical factors involved. The high PoF in the uppermost part of SMU4, despite having a high FS, is related to the high variability of the geotechnical data in the top layer.

Within the PoF-depth profiles V5 and V7, the highest PoFs is found in SMU1. For location V5, the additional load caused by sediment accumulation since ~2,210 cal. yr BP increases the PoF from ~0.35 to 0.75. For location V7, the additional sediment load does not have a clear influence on the PoF. For all the model locations, the PoF remains close to zero in SMU3, even after an additional sediment load is applied.

Figure 10 shows colour-coded static slope stability scenarios calculated for the sediment drape at ~2,210 and ~640 cal. yr BP and for the present day on the three model transects. Generally, the highest PoF in the PoF-depth profile can be found in SMU1. Within a transect, PoFs are highest in steep zones (i.e. ~20°) with thick sediment cover on the potential

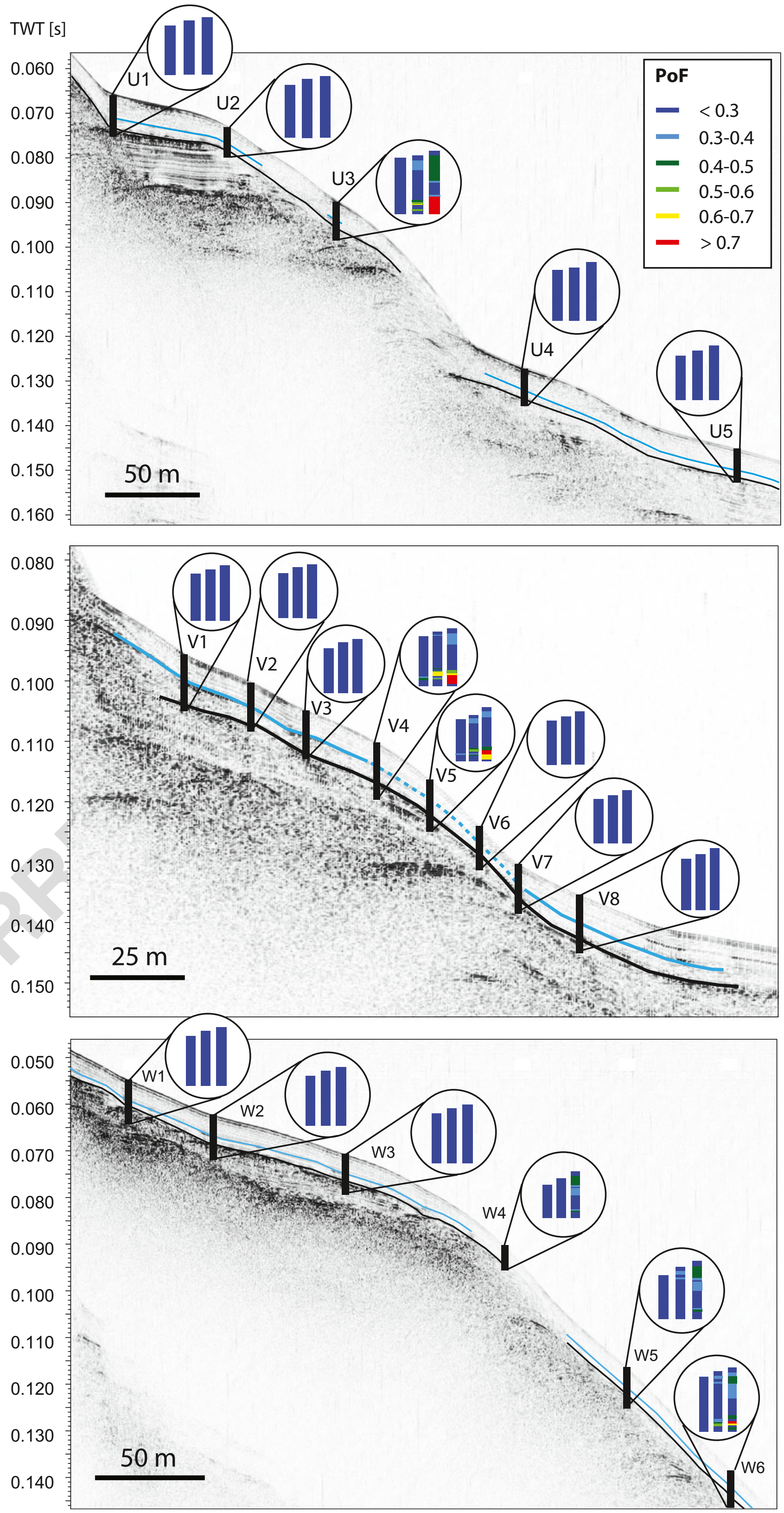

Fig. 10 Static slope stability for the three transects U, V and W (from top to bottom; see Figs. 3 and 4 for locations of transects; *black vertical lines* core locations). Magnified in circles, left: PoF for the scenario ~2,210 cal. yr BP, middle: PoF for the scenario ~640 cal. yr BP, right: PoF for present-day slope conditions. *Black and blue horizons* Strong reflections between SMU1 and 2 as well as SMU3 and 4 respectively. Seismic profile of transect V modified after Strasser and Anselmetti (2008)

failure plane. The minimum deterministic FS and maximum PoF of the FS-depth and PoF-depth profiles for each model location can be found in the electronic supplementary material (Tables ESM12 and ESM13). For the scenario ~2,210 cal. yr

BP under static loading conditions, the deterministic FS is >1 for all model locations. Only some locations on the steep slope have a PoF slightly greater than 0.3 (U3: 0.38, V4: 0.43, V5: 0.33). For the ~640 cal. yr BP scenario under static loading conditions, locations U3, V4, V5 and W6 have a deterministic minimum FS of ≤1 in SMU1; for all the other model locations, the minimum FS is >1. On transect U, all PoFs except for U3 (0.63) are <0.2. On transect V, PoFs are <0.3 for all model locations except for V4 (PoF: 0.66) and V5 (PoF: 0.59). PoFs for transect W are <0.3 for SMU1 of all the locations except for W6 (PoF: 0.55). For the present-day situation, the minimum FS values range from 0.86 (V4) to 3.15 (U5). U3, V4, V5 and W6 have FS values <1, which implies that the slope is unstable at these locations in a deterministic analysis. In a probabilistic analysis, the maximum PoFs are 0.82 (U3), 0.83 (V4), 0.75 (V5) and 0.73 (W6), suggesting a high probability of static slope instability at these model locations for the present-day slope conditions. Locations W4 (PoF: 0.42) and W5 (PoF: 0.45) show medium probabilities of failure. The PoF of the relatively flat zones (slope gradient ~5–10°), however, is relatively low for the present-day sediment drape (i.e. <0.3). Since S2 occurred (~2,210 cal. yr BP), additional sediment loading has doubled the PoF for the locations in the steep zones.

In summary, back analyses of S2 show low PoFs under static loading conditions, whereas back analyses of S3 reveal that some of the locations with steep slope gradients show a slightly increased PoF. Thus, within ~1,570 years between the two events, the static slope stability decreased. This implies a higher failure susceptibility when subjected to additional trigger mechanisms.

Critical pseudostatic accelerations for past subaqueous landslides

The a_c values required for the triggering of S2 and S3 are listed per model location in Table 3. For the sediment drape at ~2,210 cal. yr BP, the minimum a_c is found at locations U3 and V4 (both 0.01g), V5 (0.04g) and W6 (0.05g). For the scenario ~640 cal. yr BP, the minimum a_c is 0 for U3, V4, V5 and W6, suggesting that no additional force is needed to cause failure at these model locations. Model location W5, situated in the same water depth as the failure scar of the slide, needs a minimum a_c of 0.04g.

Discussion

Interpretation of glide-plane characteristics based on sediment core data

From the observations that LU3c (for S1a) and LU3b (for S2 and S3) directly overlie LU1, and from the geomorphic expression of slide translation areas, it is inferred that the glide plane (cf. blue arrow in Fig. 6) of the three landslides is located in LU1 (late glacial plastic muds). Macroscopic and

Table 3 Pseudostatic critical accelerations (a_c) and depth of minimum a_c for the model locations

Location	Slope gradient (°)	Min. a_c 2,210 cal. yr BP (×g)	Depth of min. a_c in a_c-depth profile (m)	Min. a_c 640 cal. yr BP (×g)	Depth of min. a_c in a_c-depth profile (m)
U1	4.2	0.18	5.67	0.16	6.40
U2	11.2	0.16	4.58	0.13	4.57
U3	18.0	0.02	4.52	0	5.25
U4	10.1	0.13	4.90	0.10	5.62
U5	5.2	0.26	4.25	0.22	4.97
V1	9.1	0.11	4.92	0.08	5.64
V2	10.0	0.17	4.20	0.12	4.92
V3	10.0	0.16	4.14	0.12	4.86
V4	18.2	0.01	4.64	0	5.36
V5	19.9	0.04	3.88	0	4.60
V6	12.0	0.17	3.52	0.12	4.24
V7	9.8	0.20	3.67	0.16	4.39
V8	8.3	0.15	5.10	0.13	5.82
W1	8.1	0.13	5.66	0.11	6.38
W2	5.2	0.20	5.88	0.18	6.57
W3	6.0	0.24	4.76	0.21	5.48
W4	20.5	0.13	3.09	0.06	3.80
W5	18.3	0.10	3.77	0.04	4.49
W6	20.4	0.05	3.92	0	4.65

JrnlID 367_ArtID 492_Proof# 1 - 06/01/2017

geotechnical data indicate that the location of the glide planes within LU1 varies between the investigated subaqueous landslides. For S1a and S2, the glide plane is located in LU1a, whereas for S3 the glide plane is located in LU1b/c, close to the transition to LU2.

The cores taken along a transect on S1a (Fig. 6a) may contain some information about the slide mechanism: from the undisturbed part of LU1 in the topmost core, it is inferred that the original sediment cover (top of LU1, LU2, LU3a and large parts of LU3b) sled completely downslope, i.e. without parts of the slide being redeposited at that location. For core ZH15-S10(II), however, the change in lamination angles within the late glacial plastic muds (cf. dashed white line in Fig. 6a) may be interpreted as the location of the glide plane, which is covered by the 'tail' of the landslide. The succession in core ZH15-S11 is interpreted as being clasts of LU3 mixed with LU1 during the slide in the lower part of the slope.

Slope stability evaluation

Location of failure initiation

Lacustrine chalks, such as those found in LU3 (correlating with SMU3), are described in the literature as 'structure-sensitive' (i.e. their matrix can fall apart suddenly upon shaking; e.g. Huder 1963; Schindler 1996), and have been documented as 'weak layers' causing landslides that slide on a slurry rather than on a distinct glide plane (e.g. landslides of Zug; Schindler and Gyger 1989; Schindler 1996). On the slopes of Oberrieden, however, the modelled critical failure plane is found in SMU1 for the back-calculated and present-day scenarios. Lithologically, the modelled glide plane corresponds to the LU1 (late glacial plastic muds; Fig. 6). The modelled results thus coincide with the observed results from sediment cores taken on the failure planes. The reason why the failure develops in SMU1 (or, from a lithological point of view, why the late glacial plastic muds favour slope instability) may be found in the different mechanical behaviour of SMU1 in contrast to its covering mechanical units (i.e. the relatively low s_u compared to that of the covering SMU2). Such a different mechanical behaviour may be explained by the mineralogical composition (e.g. Hein and Longstaffe 1985; Stegmann et al. 2007). Mineralogical measurements by Gyger et al. (1976) on the late and postglacial sediments in Lake Zurich showed a much higher clay content in the late glacial clays compared to the overlying lithological units. Also for other lacustrine or marine slopes, clay often represents weak layers (Laberg et al. 2003; Solheim et al. 2005; Dan et al. 2007; Stegmann et al. 2007; Strasser et al. 2007; Sultan et al. 2010).

Interestingly, the modelled critical failure plane is not located at the transition between two SMUs, but rather within SMU1. The exact determination of whether the glide plane is located in LU1a or LUb/c is not possible in the model, as the two lithological subunits belong to the same SMU. The reason why slide S3 has its glide plane in a higher lithological subunit (LU1 b/c) than S1a and S2 (LU1a) may be related to the slope geometry: as the failure scar of S3 is located within a steep zone (and not at the top of a steep zone as for S1a and S2; cf. Results section), the additional downward-driving forces of the sediment columns in the upslope neighbourhood may be responsible for a slightly higher location of the weakest zone within the mechanic stratigraphy for S3.

The downslope position of the headscarp can be identified quite accurately: the location with the highest overall values in the PoF-depth profile corresponds to the position of the headscarp in the slope, identified from the DDM. This can be well identified at the locations U3, V4 and W5/W6. Kohv et al. (2009) concluded from an SSA on subaerial slopes that the critical slope angle for failure of groundwater-saturated glaciolacustrine clays is >10°. The locations of the failure scars in the present study area show similar results for the sublacustrine slopes in Lake Zurich. Also for Lake Lucerne, the majority of the slides in the late glacial clays occur on slopes >10° (Schnellmann et al. 2006; Strasser et al. 2011).

The question why the patches between the three subaqueous landslides in the study area have not (yet) failed is of importance. The slope gradient of the potential glide plane and the spatial sediment-mechanical unit thicknesses distribution must influence the lateral extension of the slides. Although the present approach allows the determination of the glide plane and the identification of potential future headscarp locations, it is difficult to assess the lateral extension of the landslides.

Static and pseudostatic stability of the Oberrieden slopes

As for Lake Lucerne (Strasser et al. 2007), the static stability conditions of the Oberrieden slopes can change over short geological timescales. At the time of the occurrence of the past slides, the yet unfailed slopes were statically more stable than for the present-day situation. The more sediment accumulates with time, the higher the static load, and thus the lower an external force needed to create slope failure.

The results of the present study (Fig. 10) indicate that the Oberrieden slope was statically stable when S2 occurred. Hence, an external force must have triggered S2. This supports other evidence of that slide being earthquake-triggered, as suggested by Strasser and Anselmetti (2008) based on a geotechnical approach. a_c of 0.04 and 0.05g were needed to cause failure at the weakest model locations of the V and W transects. For Lake Lucerne, Strasser et al. (2011) approximate a minimum a_c of 0.034g for the ~2,200 cal. yr BP event and relate this value to the probably strongest Holocene regional earthquake. The slightly higher a_c values of the present study indicate thus a marginally higher shaking intensity for

Lake Zurich. For the scenario ~640 cal. yr BP, the model locations on steep slope gradients (i.e. ~20°) are statically slightly unstable both for the deterministic and probabilistic model, whereas the modelled locations on the smaller slope gradients (i.e. ~5–10°) are stable. On transect W, which is closest to S3, minimal a_c neighbouring the slide extent must be in the range between 0 (W6) and 0.04g (W5). S3 may be related to the historical 1356 AD Basel earthquake, which might have had a maximum intensity of VI in Zurich (Schwarz-Zanetti and Fäh 2011). It is assumed that the slope was already in a 'labile' situation, which might have allowed an earthquake intensity of <VI to trigger a failure. The back-analysed a_c should be used only as a first-order estimation, as the buttressing effect at the toe of the steep zones is not included. The steeper parts of the slope (~20°) with high PoFs are prone to failure, even without external trigger, as they are 'charged with sediment'.

The undulations that are located where the highest PoF in the V transect has been modelled (Fig. 4b) might be a geomorphic expression of a local instability, indicating some pre-failure movements as first stage of landslides (e.g. Leroueil et al. 1996; Shillington et al. 2012). The formation by waves can be ruled out, as the features are located between ~80 and ~90 m water depth, much deeper than the wave base. Sediment undulations have also been interpreted as formed by bottom currents or hyperpycnal flows (e.g. Bornhold and Prior 1990; Mosher and Thomson 2002; Urgeles et al. 2007). Bottom currents often create sediment waves that are oblique to the bathymetric contours (e.g. Flood et al. 1993). Here, the undulations are parallel to the bathymetric contours. Hyperpycnal flows are also unlikely, as there is no major river inflow nearby that could generate excess density by its sediment load (e.g. Parsons et al. 2001). As the undulations coincide with the location of the highest PoF in the transect, it is interpreted that the slope is unstable at some particular locations, which results in these features, yet it is not weak enough to slide completely. Little additional force may be needed to trigger a subaqueous landslide in the study area. However, as large parts of the slope have already failed, only relatively small undisturbed sediment patches may be mobilized.

The stability of the slope at the time of the S1a occurrence must have been very similar to the stability for the present-day situation, as in the ~100 years since the landslide occurrence only ~10–20 cm of sediment accumulated on the glide plane. In 1917, a wooden construction for changing booths of a new public bath was installed at the shore (pers. comm. I. Raimann, village of Oberrieden). The construction may have provided the extra load on the sediment to cause the slope to fail. As the translation areas of S1a and S1b are not connected, it is not clear whether these slides were triggered synchronously. S1b may have been triggered by construction activity onshore and, by adding its deposit on the slope above the main slide's headscarp, may have acted as an additional force for triggering S1a. Another explanation is that S1b was triggered independently in 1965, when a landfill occurred in the near-shore area (pers. comm. I. Raimann, village of Oberrieden) to extend the public baths (located in the immediate vicinity of the S1b failure scar). The exact slide mechanism, however, remains unknown.

Limitations and quality of the modelling approach

Considering the irregular geometry of the slope in the study area, the assumption of the infinite-slope model that the glide plane is planar is not strictly valid. However, for a SSA at single model locations, the model is not affected. If spatial SSAs are conducted, the buttressing effects of interslice forces need to be considered. Furthermore, the simple model of the present study does not include any considerations of hydrological effects. However, it is considered that this is not relevant in this case, as no rivers inflow the study area and no fluid flow evidence can be found in the geoacoustic datasets.

A linear increase in ρ_{bulk} and s_u values used in many SSAs may give reliable results for the investigation of slopes with homogeneous lithological units. For slopes with small-scale (i.e. decimetre) variations of mechanical properties with depth, as in the Oberrieden case, profiles instead of gradients might be more appropriate.

Although the present concept expresses slope stability quantitatively, the computed PoFs on the slopes in the study area should not be interpreted as absolute values but should rather be regarded relative to other modelled PoFs. However, if interpreted with geological understanding, the concept yields valuable information. Formally, the calculated a_c on the unfailed slopes are to be regarded as maximum values. However, it is assumed that the stability conditions in the pre-failure areas were similar to the ones on the transects. This implies that values of minimal a_c must have been very close to the maximal a_c.

The comparison of the present results to those from calculations with SLIDE for transect V shows that the simple model of this study provides useful data for determination of the position of the failure plane within the sediment column (see electronic supplementary material Figs. ESM1 and ESM2): the potential glide plane modelled with SLIDE is also located in LU1. The global mean deterministic and probabilistic FS (1.36 and 1.47) does not exclude single locations in the transect with a smaller FS. By the use of gradients in the SLIDE model, variations in geotechnical parameters are smoothed out.

The present approach does not explain why the patches between the slides have not failed. A spatial analysis may help determining the lateral extent of the subaquatic landslides. Also, the limit-equilibrium approach does not give any results about the mechanism of the failure initiation. An approach that treats failure as a shear-band propagation process, such as applied by Puzrin and Germanovich (2005), would be necessary.

Conclusions

The presented concept provides a suitable tool for assessing the stability of subaqueous slopes. The high density of the sediment cores and CPT sites in a well-investigated area and the high-resolution measurement of the geotechnical parameters allow the inclusion of spatial variability in the model. To the authors' knowledge, the concept of including an adaptable sediment-mechanical stratigraphy into a limit-equilibrium SSA has not been applied on a larger scale. The concept thus might be an important contribution to the SSA for an entire lake basin or stretch of continental margin (excluding gas-rich littoral deposits or deltas). To this end, a bathymetric and seismic reflection dataset, and a grid of homogeneously distributed depth-profiles of bulk density and undrained shear strength on the undisturbed lateral slopes are needed. If the subsurface properties of a whole lake basin or stretch of the continental margin vary considerably (e.g. provoked by varying detrital input from major rivers), the slope may be divided into different zones, each with similar properties. Hence, if applied on a larger scale, as a first step, general patterns of geotechnical profiles taken at a low spatial sampling resolution (e.g. one core and one CPT profile per km^2) may be detected to construct zones. As a second step, the spatial sampling resolution can be increased and mechanical stratigraphies for the different zones can be constructed.

Extended from a 1D approach to a spatial basin-wide approach, the concept is expected to yield information on failure-prone zones with simple, time-efficient methods. Failure-prone zones can in a further step be analysed for their tsunamigenic potential. The main findings of this study can be summarised as follows:

1. The glide plane of the three investigated subaqueous slides in Lake Zurich can be assigned to late glacial plastic muds, both from modelled results and sedimentological groundtruthing. The glide plane is thus located in the same lithostratigraphic unit as documented for nearby Lake Lucerne (Strasser et al. 2007).
2. The location of the headscarp of historical and prehistorical subaqueous landslides corresponds to the model locations in the transects with the highest probabilities of failure. This approach to assess slope stability should thus be able to determine the headscarp locations of future landslides.
3. The model supports the hypothesized earthquake triggers for the ~2,210 and ~640 cal. yr BP events from a geotechnical point of view and adds first quantitative constraints for critical pseudostatic earthquake accelerations for Lake Zurich.
4. Today, sediment-charged, steeper (i.e. ~20°) slopes in the study area are prone to failure, even without the need of an additional trigger. Modelled results imply that future subaqueous landslides in Lake Zurich may glide in late glacial plastic muds (LU1)—hence, in the same lithological unit as the three investigated slides occurring in the past.

Acknowledgements This work was supported by the Swiss National Foundation Grant Nr. 133481. We thank Anna Reusch, Katrina Kremer, Stefano Fabbri, Robert Hofmann, Reto Seifert, Stewart Bishop, Christian Zoellner, Tobias Schwestermann and Utsav Mannu for their efforts during the data acquisition, Andrea Wolter for her inputs with SLIDE Software, and Beat Rick (GeoVonMoos AG) for the access to additional Lake Zurich data. Gratefully acknowledged are two anonymous reviewers and the editors for their constructive inputs.

Compliance with ethical standards

Conflict of interest The authors declare that there is no conflict of interest with third parties.

References

Abramson LW, Lee TS, Sharma S, Boyce GM (2002) Slope stability and stabilization methods, 2nd edn. Wiley, New York

Biscontin G, Pestana JM (2006) Factors affecting seismic response of submarine slopes. Nat Hazards Earth Syst Sci 6:97–107. doi:10.5194/nhess-6-97-2006

Bitterli T, George M, Matousek F, Christe R, Brändli R, Frey D (2004) Grundwasservorkommen. In: Hydrologischer Atlas der Schweiz, Tafel 8.6. Bundesamt für Umwelt, Bern

Blum P (1997) Physical properties handbook, ODP Tech Note 26. doi:10.2973/odp.tn.26.1997

Bornhold B, Prior DB (1990) Morphology and sedimentary processes on the subaqueous Noeick River delta, British Columbia, Canada. In: Colella A, Prior DB (eds) Coarse-grained deltas. Blackwell, Oxford, pp 169–181

Chandler DS (1996) Monte Carlo simulation to evaluate slope stability. In: Shakelford C, Nelson PP, Roth MJS (eds) Uncertainty in the geologic environment: from theory to practice. American Society of Civil Engineers, New York, pp 474–493

Chapron E, Van Rensbergen P, De Batist M, Beck C, Henriet JP (2004) Fluid-escape features as a precursor of a large sublacustrine sediment slide in Lake Le Bourget, NW Alps, France. Terra Nov. 16: 305–311. doi:10.1111/j.1365-3121.2004.00566.x

Coduto DP, Yeung MR, Kitch WA (2011) Geotechnical engineering: principles and practices, 2nd edn. Prentice Hall, Upper Saddle River

Craig RF (2004) Craig's soil mechanics, 7th edn. Spon Press, New York

Dan G, Sultan N, Savoye B (2007) The 1979 Nice harbour catastrophe revisited: trigger mechanism inferred from geotechnical measurements and numerical modelling. Mar Geol 245:40–64. doi:10.1016/j.margeo.2007.06.011

Giovanoli F (1979) Die remanente Magnetisierung von Seesedimenten. PhD Thesis Nr. 6350, ETH Zürich

Gyger M, Müller-Vonmoos M, Schindler C (1976) Untersuchungen zur Klassifikation spät- und nacheiszeitlicher Sedimente aus dem Zürichsee. Schweiz Mineral Petrogr Mitt 56:387–406

Heim A (1876) Bericht und Expertengutachten über die im Februar und September 1875 in Horgen am Zürichsee vorgekommenen Rutschungen. Die Eisenbahn 4:191–196

Hein FJ, Longstaffe FJ (1985) Sedimentologic, mineralogic, and geotechnical descriptions of fine-grained slope and basin deposits, Baffin Island Fiords. Geo-Mar Lett 5:11–16. doi:10.1007/BF02629791

Huder J (1963) Bestimmung der Scherfestigkeit strukturempfindlicher Böden unter besonderer Berücksichtigung der Seekreide. Mitt Versuchsanstalt Wasserbau Erdbau Eidgenössischen Tech Hochschule Zürich 58:1–35

Jiang L, Leblond PH (1992) The coupling of a submarine slide and the surface. J Geophys Res 97:12731–12744

Jibson RW (1993) Predicting earthquake-induced landslide displacements using Newmark's sliding block analysis. Transp Res Rec 1411:9–17

Jibson RW (2012) Models of the triggering of landslides during earthquakes. In: Clague JJ, Stead D (eds) Landslides: types, mechanisms and modeling. Cambridge University Press, Cambridge, pp 196–206. doi:10.1017/CBO9780511740367.018

Johari A, Javadi AA (2012) Reliability assessment of infinite slope stability using the jointly distributed random variables method. Sci Iran 19:423–429. doi:10.1016/j.scient.2012.04.006

Kelts K (1978) Geological and sedimentary evolution of Lakes Zurich and Zug, Switzerland. PhD Thesis Nr. 6146, ETH Zurich

Kelts K, Hsü KJ (1980) Resedimented facies of 1875 Horgen slumps in Lake Zurich and a process model of longitudinal transport of turbidity currents. Eclogae Geol Helv 73:271–281

Kelts K, Briegel U, Ghilardi K, Hsu K (1986) The limnogeology-ETH coring system. Swiss J Hydrol 48:104–115. doi:10.1007/BF02544119

Klaucke I, Cochonat P (1999) Analysis of past seafloor failures on the continental slope off Nice (SE France). Geo-Mar Lett 19:245–253

Kohv M, Talviste P, Hang T, Kalm V, Rosentau A (2009) Slope stability and landslides in proglacial varved clays of western Estonia. Geomorphology 106:315–323. doi:10.1016/j.geomorph.2008.11.013

Kramer SL (1996) Geotechnical earthquake engineering. Prentice-Hall, Upper Saddle River

Laberg J, Vorren TO, Mienert J, Haflidason H, Bryn P, Lien R (2003) Preconditions leading to the Holocene Trænadjupet Slide. In: Submarine mass movements and their consequences, vol 19. Springer, Heidelberg, pp 247–254

Lacasse S, Nadim F (1996) Uncertainties in characterising soil properties. In: Shackelford CD, Nelson PP, Roth MJS (eds) Uncertainty in the geologic environment: from theory to practice. American Society of Civil Engineers, New York, pp 49–75

Leroueil S, Vaunat J, Picarelli L, Locat J, Lee H, Faure R (1996) Geotechnical characterisation of slope movements. In: Senneset K (ed) Landslides, 1st edn. Balkema, Rotterdam, pp 53–74

Leynaud D, Sultan N (2010) 3-D slope stability analysis: a probability approach applied to the Nice slope (SE France). Mar Geol 269:89–106. doi:10.1016/j.margeo.2009.12.002

Leynaud D, Mienert J, Nadim F (2004) Slope stability assessment of the Helland Hansen area offshore the mid-Norwegian margin. Mar Geol 213:457–480. doi:10.1016/j.margeo.2004.10.019

Lister GS, Giovanoli F, Eberli G, Finckh P, Finger W, He Q, Heim C, Hsü KJ, Kelts K, Peng C, Sidler C, Zhao X (1984) Late Quaternary sediments in Lake Zurich, Switzerland. Environ Geol 5:191–205

Locat J, Lee HJ (2002) Submarine landslides: advances and challenges. Can Geotech J 39:193–212. doi:10.1139/t01-089

Lunne T, Robertson PK, Powell JJM (2002) Cone penetration testing in geotechnical practice, 2nd edn. Spon Press, London

Masson DG, Harbitz CB, Wynn RB, Pedersen G, Løvholt F (2006) Submarine landslides: processes, triggers and hazard prediction. Philos Trans A Math Phys Eng Sci 364:2009–2039. doi:10.1098/rsta.2006.1810

Morgenstern NR, Price VE (1967) A numerical method for solving the equations of stability of general slip surfaces. Comput J 9:388–393

Mosher DC, Thomson RE (2002) The Foreslope Hills: large-scale, fine-grained sediment waves in the Strait of Georgia, British Columbia. Mar Geol 192:275–295. doi:10.1016/S0025-3227(02)00559-5

Nadim F, Einstein H, Roberds W (2005) Probabilistic stability analysis for individual slopes in soil and rock. In: Hungr O, Fell R, Couture R, Eberhard E (eds) Landslide risk management. Taylor & Francis, Boca Raton, p 764

Newmark NM (1965) Effects of earthquakes on dams and embarkments. Geotechnique 2:139–160

Nipkow F (1927) Über das Verhalten der Skelette planktischer Kieselalagen im geschichteten Tifenschlamm des Zürich- und Baldeggersees. PhD Thesis Nr. 455, ETH Zurich

Parsons JD, Bush JWM, Syvitski JPM (2001) Hyperpycnal plume formation from riverine outflows with small sediment concentrations. Sedimentology 48:465–478. doi:10.1046/j.1365-3091.2001.00384.x

Prior DB, Coleman JM, Bornhold BD (1982) Results of a known seafloor instability event. Geo-Mar Lett 2:117–122. doi:10.1007/BF02462751

Schindler C (1974) Zur Geologie des Zürichsees. Eclogae Geol Helv 67:163–196

Schindler C (1976) Eine geologische Karte des Zürichsees und ihre Deutung. Eclogae Geol Helv 69:125–138

Schindler CM (1996) Aussergewöhnliche Rutschungen, Felsstürze und Murgänge. In: Instabile Hänge und andere risikorelevante natürliche Prozesse. Birkhäuser, Basel, pp 73–84

Schindler C, Gyger M (1989) The landslides of Zug seen 100 years after the analysis of Albert Heim. In: Bonnard C (ed) Rutschungsphänomene im Gebiet des Alpenbogens. Balkema, Rotterdam, pp 123–126

Schlüchter C (1984) Geotechnical properties of Zübo sediments. In: Hsü KJ, Kelts K (eds) Quaternary geology of Lake Zurich: an interdisciplinary investigation by deep-lake drilling. Schweizerbart, Stuttgart, pp 135–140

Schnellmann M, Anselmetti FS, Giardini D, McKenzie JA, Ward SN (2002) Prehistoric earthquake history revealed by lacustrine slump deposits. Geology 30:1131–1134. doi:10.1130/0091-7613(2002)030<1131:PEHRBL>2.0.CO;2

Schnellmann M, Anselmetti FS, Giardini D, McKenzie JA (2005) Mass movement-induced fold-and-thrust belt structures in unconsolidated sediments in Lake Lucerne (Switzerland). Sedimentology 52:271–289. doi:10.1111/j.1365-3091.2004.00694.x

Schnellmann M, Anselmetti FS, Giardini D, McKenzie JA (2006) 15,000 years of mass-movement history in Lake Lucerne: implications for seismic and tsunami hazards. Eclogae Geol Helv 99:409–428. doi:10.1007/s00015-006-1196-7

Schwarz-Zanetti G, Fäh D (2011) Grundlagen des Makroseismischen Erdbebenkatalogs der Schweiz Band 1:1000–1680. vdf Hochschulverlag AG, Zürich

Shillington DJ, Seeber L, Sorlien CC, Steckler MS, Kurt H, Dondurur D, Çifçi G, Imren C, Cormier MH, McHugh CMG, Gürçay S, Poyraz D, Okay S, Atgin O, Diebold JB (2012) Evidence for widespread creep on the flanks of the sea of Marmara transform basin from marine geophysical data. Geology 40:439–442. doi:10.1130/G32652.1

Solheim A, Bryn P, Sejrup HP, Mienert J, Berg K (2005) Ormen Lange - An integrated study for the safe development of a deep-water gas field within the Storegga Slide Complex, NE Atlantic continental margin; executive summary. Mar Pet Geol 22:1–9. doi:10.1016/j.marpetgeo.2004.10.001

Stegmann S, Mörz T, Kopf A (2006a) Initial results of a new free fall-cone penetrometer (FF-CPT) for geotechnical in situ characterisation of soft marine sediments. Nor Geol Tidsskr 86:199–208

Stegmann S, Villinger H, Kopf A (2006b) Design of a modular, marine free-fall cone penetrometer. Sea Technol 47(02):27–33

Stegmann S, Strasser M, Anselmetti F, Kopf A (2007) Geotechnical in situ characterization of subaquatic slopes: the role of pore pressure transients versus frictional strength in landslide initiation. Geophys Res Lett. doi:10.1029/2006GL029122

Steiner A (2013) Stability of submarine slope sediments using dynamic and static piezocone penetrometers. Doctoral Thesis, Bremen University

Steiner A, L'Heureux J-S, Kopf A, Vanneste M, Longva O, Lange M, Haflidason H (2012) An in-situ free-fall piezocone penetrometer for characterizing soft and sensitive clays at Finneidfjord (northern Norway). In: Submarine Mass Movements and Their Consequences, vol 31. Springer, Heidelberg, pp 99–109. doi:10.1007/978-1-4020-6512-5

Strasser M, Anselmetti FS (2008) Mass-movement event stratigraphy in Lake Zurich; a record of varying seismic and environmental impacts. Beiträge Geol Schweiz 95:23–41

Strasser M, Anselmetti FS, Fäh D, Giardini D, Schnellmann M (2006) Magnitudes and source areas of large prehistoric northern Alpine earthquakes revealed by slope failures in lakes. Geology 34:1005. doi:10.1130/G22784A.1

Strasser M, Stegmann S, Bussmann F, Anselmetti FS, Rick B, Kopf A (2007) Quantifying subaqueous slope stability during seismic shaking: Lake Lucerne as model for ocean margins. Mar Geol 240:77–97. doi:10.1016/j.margeo.2007.02.016

Strasser M, Schindler C, Anselmetti FS (2008) Late Pleistocene earthquake-triggered moraine dam failure and outburst of Lake Zurich, Switzerland. J Geophys Res Earth Surf 113:1–16. doi:10.1029/2007JF000802

Strasser M, Hilbe M, Anselmetti FS (2011) Mapping basin-wide subaquatic slope failure susceptibility as a tool to assess regional seismic and tsunami hazards. Mar Geophys Res 32:331–347. doi:10.1007/s11001-010-9100-2

Strasser M, Monecke K, Schnellmann M, Anselmetti FS (2013) Lake sediments as natural seismographs: a compiled record of Late Quaternary earthquakes in Central Switzerland and its implication for Alpine deformation. Sedimentology 60:319–341. doi:10.1111/sed.12003

Strupler M, Hilbe M, Anselmetti FS, Strasser M (2015) Das neue Tiefenmodell des Zürichsees: Hochauflösende Darstellung der geomorphodynamischen Ereignisse im tiefen Seebecken. Swiss Bull Angew Geol 20:71–83

Sultan N, Savoye B, Jouet G, Leynaud D, Cochonat P, Henry P, Stegmann S, Kopf A (2010) Investigation of a possible submarine landslide at the Var delta front (Nice slope - SE France). Can Geotech J 47:486–496. doi:10.1139/T09-105

Tappin DR, Watts P, McMurtry GM, Lafoy Y, Matsumoto T (2001) The Sissano, Papua New Guinea tsunami of July 1998 - Offshore evidence on the source mechanism. Mar Geol 175:1–23. doi:10.1016/S0025-3227(01)00131-1

Tobutt DC (1981) Monte Carlo simulation methods for slope stability. Comput Geosci 8:199–208

Urgeles R, De Mol B, Puig P, De Batist M, Hughes-Clarke JE (2007) Sediment undulations on the Llobregat prodelta: signs of early slope instability or sedimentary bedforms? J Geophys Res 112:1–12. doi:10.1029/2005JB003929

Wolff T (1996) Probabilistic slope stability in theory and practice. In: Uncertainty in the geologic environment. ASCE, pp 419–433

Zandbergen PA (2011) Error propagation modeling for terrain analysis using dynamic simulation tools in ArcGIS Modelbuilder. In: Hengl T, Evans IS, Wilson JP, Gould M (eds) Geomorphometry 2011. Redlands, pp 57–60

AUTHOR QUERIES

AUTHOR PLEASE ANSWER ALL QUERIES.

Q1. “Flood et al. 1993” is cited in text but not given in the reference list. Please provide details in the list or delete the citation from the text.

Q2. “Puzrin and Germanovich (2005)” is cited in text but not given in the reference list. Please provide details in the list or delete the citation from the text.